# Dark Photon Dark Matter and Low-frequency Gravitational-wave Detection with Gaia-like Astrometry

Haipeng An[1,2,3], Tingyu Li[1], Jing Shu[3,4,5], Xin Wang[4,6], Xiao Xue[7,8] , and Yue Zhao[9]

[1] Department of Physics, Tsinghua University, Beijing 100084, People's Republic of China; anhp@mail.tsinghua.edu.cn, lity22@mails.tsinghua.edu.cn

[2] Center for High Energy Physics, Tsinghua University, Beijing 100084, People's Republic of China

[3] Center for High Energy Physics, Peking University, Beijing 100871, People's Republic of China; jshu@pku.edu.cn

[4] School of Physics and State Key Laboratory of Nuclear Physics and Technology, Peking University, Beijing 100871, People's Republic of China; xin.wang@soton.ac.uk

[5] Beijing Laser Acceleration Innovation Center, Huairou, Beijing 101400, People's Republic of China

[6] School of Physics and Astronomy, University of Southampton, Southampton, SO17 1BJ, UK

[7] II. Institute of Theoretical Physics, Universität Hamburg, 22761 Hamburg, Germany; xiao.xue@desy.de

[8] Deutsches Elektronen-Synchrotron DESY, Notkestr. 85, 22607 Hamburg, Germany

[9] Department of Physics and Astronomy, University of Utah, Salt Lake City, UT 84112, USA; zhaoyue@physics.utah.edu

## Abstract

Astrometric surveys offer us a method for searching for elusive cosmic signatures, such as ultralight dark photon dark matter and gravitational waves (GWs), by observing the temporal change of stars' apparent locations. The detection capabilities of such surveys rapidly decrease at low frequencies, because the signals become hardly distinguishable from the background motion of stars. In this work, we find that the background motion can be well described by a linear model over time, based on which we propose a linear background subtraction scheme. Compared to the conventional quadratic subtraction, the advantage of linear subtraction emerges within the frequency range below $6 \times 10^{-9}$ Hz. Taking dark photons with purely gravitational interactions, dark photons with additional $U(1)_B$ or $U(1)_{B-L}$ gauge interactions, and low-frequency GWs as examples, we illustrate that the linear subtraction scheme can result in an enhancement of more than 1 order of magnitude in the exclusion limits of Gaia-like experiments in the low-frequency range.

## 1. Introduction

The development of astrophysical observation methods has revolutionized our understanding of the cosmos, enabling us to probe subtle effects induced by new astrophysical sources or new physics with unprecedented precision. Recently, several Pulsar Timing Array (PTA) collaborations reported the first evidence for the stochastic gravitational-wave (GW) background at nanohertz frequencies (B. Allen 1996; G. Agazie et al. 2023a; J. Antoniadis et al. 2023; D. J. Reardon et al. 2023; H. Xu et al. 2023), which may arise from a population of inspiraling supermassive black hole binaries (A. Sesana et al. 2008).

Apart from the GW signals, PTA experiments can also probe several new physics models. One example would be ultralight bosonic dark matter (H.-Y. Schive et al. 2014; L. Hui et al. 2017), which has the potential to solve the so-called small-scale problems (D. H. Weinberg et al. 2015) of the cold dark matter model. Ultralight dark photon dark matter (DPDM) assumes that dark matter is composed of vector fields (P. Adshead & K. D. Lozanov 2021; M. A. Amin et al. 2022) with a mass around $10^{-22}$ eV. Due to its wave nature, the field value of the ultralight DPDM oscillates in an approximately coherent manner. Therefore, the ultralight DPDM can induce nontrivial oscillations of the metric due to pure gravitational effects (A. Khmelnitsky & V. Rubakov 2014; K. Nomura et al. 2020;

Y. Chen et al. 2023; J.-C. Yu et al. 2024) or impose external oscillating forces on test objects via additional $U(1)$ gauge interactions (A. Pierce et al. 2018), both of which can modify the pulse arrival time (A. E. Nelson & J. Scholtz 2011; N. K. Porayko et al. 2018; Y.-M. Wu et al. 2022; X. Xue et al. 2022; A. Afzal et al. 2023; Z.-Q. Xia et al. 2023; D. Chowdhury et al. 2024).

The GW or DPDM background can also result in the deflection of light emitted from astrophysical objects to the Earth due to the following two distinct effects:

1. GWs or DPDM with purely gravitational interactions can induce metric perturbations, which can affect the trajectory of the light emitted from the sources (V. B. Braginsky et al. 1990; T. Pyne et al. 1996; N. Kaiser & A. Jaffe 1997; S. M. Kopeikin et al. 1999; L. G. Book & E. E. Flanagan 2011). As a result, the apparent positions of the stars we observe slightly deviate from their initial positions. Such displacements depend on metric perturbations at both the Earth and stars, while the Earth term should be dominant, as we will explain later. It should also be mentioned that, unlike the deflection induced by ultralight scalar dark matter, which is suppressed due to an approximate spherical symmetry, the deflection caused by DPDM is generally not suppressed (Y. Chen et al. 2023).

2. DPDM coupling to the baryon number $U(1)_B$ or the baryon number minus the lepton number $U(1)_{B-L}$ can lead to the aberration effect, which also changes the apparent position of stars (H.-K. Guo et al. 2019).

By precisely measuring the variation of stars' apparent positions, it is hoped that traces of GW and DPDM signals can be captured in the Gaia mission (T. Prusti et al. 2016) and upcoming astrometric surveys like Roman (Y. Wang et al. 2021, 2022; Z. Haiman et al. 2023; K. Pardo et al. 2023) and Theia (C. Boehm et al. 2017; J. Garcia-Bellido et al. 2021; F. Malbet et al. 2021). Gaia observes the positions, proper motions, and parallaxes of more than $10^9$ objects with unprecedented accuracy (T. Prusti et al. 2016). The sensitive frequency of Gaia is determined by its survey lifetime $T_{obs} = 10$ yr and observational cadence $\Delta t = 24$ days, typically $10^{-9}$ Hz $\lesssim f \lesssim 10^{-7}$ Hz. Hence, Gaia can provide complementary detection capabilities to PTA experiments for nanohertz astrophysical sources (C. J. Moore et al. 2017; D. Bini & A. Geralico 2018; J. Darling et al. 2018; S. A. Klioner 2018; D. P. Mihaylov et al. 2018; L. O'Beirne & N. J. Cornish 2018; H.-K. Guo et al. 2019; W. Qin et al. 2019, 2021; D. P. Mihaylov et al. 2020; S. Aoyama et al. 2021; S. Jaraba et al. 2023; M. Çalışkan et al. 2024; Q. Liang et al. 2024).

To extract the deflections of the apparent positions of stars caused by external signals, we need to subtract their intrinsic background motion stemming from the physical motion of stars with respect to the solar barycenter and the secular aberration due to the moving reference system. This intrinsic motion can induce large angular deflection far exceeding the resolution of Gaia. For signals with frequencies $f \gtrsim 2/T_{obs} \sim 6 \times 10^{-9}$ Hz, the background subtraction essentially does not influence the sensitivity, since the oscillation pattern of GWs or DPDM is distinct from the background. Conversely, if $f \lesssim 6 \times 10^{-9}$ Hz, a half-oscillating cycle would not be observable in the time-series data within the operational lifetime of Gaia. In such cases, the signal is also partially subtracted, thereby reducing the sensitivity of detecting low-frequency GW and DPDM signals. Analogous to PTAs, the quadratic model is commonly used to subtract the background proper motion in the existing literature (C. J. Moore et al. 2017; H.-K. Guo et al. 2019; Y. Wang et al. 2021, 2022). However, a more comprehensive study of the background motion of stars and subtraction schemes should be implemented.

In this work, we propose a linear background subtraction scheme for the time-series data of apparent stellar positions in Gaia-like astrometric surveys. Specifically, we apply the least squares method to fit a linear function to the data, modeling the background noise. This fitted function is then subtracted from the data, effectively isolating the signal of interest. Upon analyzing the background motion of stars, we find that the impact on the apparent stellar position due to the constant acceleration from the galactic gravitational potential is negligibly small relative to Gaia's sensitivity. Meanwhile, the galactocentric acceleration of the solar barycenter mimics a linear term over time in the proper motion due to aberration. These observations serve as the primary motivation for our linear subtraction approach. Nevertheless, unresolvable binary systems could bring additional noise, which cannot be effectively subtracted. We provide concrete examples by calculating the astrometric deflection induced by DPDM with purely gravitational interactions while also revisiting scenarios involving DPDM with $U(1)_B$ or $U(1)_{B-L}$ gauge symmetry and GWs from binary systems. Subsequent numerical simulation using mock data reveals that our linear subtraction scheme significantly enhances Gaia's detection capabilities in the low-

frequency range, improving sensitivity by more than an order of magnitude compared to the quadratic subtraction.

The layout of this paper is as follows. In Section 2, we illustrate that the background motion of stars can be well described by a linear model over time. In Section 3, we calculate the astrometric deflections induced by GWs and DPDM. The numerical simulation and results are presented in Section 4. We summarize our main conclusions in Section 5.

## 2. Background Motion of the Apparent Stellar Locations

Astrometric objects exhibit background motion around the galactic center. Their motion is randomly distributed with a potentially nonzero expectation value, depending on the star's sky location, due to the common motion of the galactic disk. We assume that the velocity $\boldsymbol{v} = (v_r, v_\theta, v_\phi)$ in spherical polar coordinates relative to the galactic center follows a Gaussian distribution:

$$P(\boldsymbol{v}|\boldsymbol{n}) = \prod_{i=1}^{3} \frac{1}{\sqrt{2\pi}\,\sigma_{v,i}} \exp\left(\frac{(v_i - v_{0,i}(\boldsymbol{n}))^2}{2\sigma_{v,i}^2}\right), \qquad (1)$$

where $\boldsymbol{n}$ denotes the sky location of stars, $v_{0,i}(\boldsymbol{n})$ represents the expectation value of $\boldsymbol{v}$ in each direction, and $\sigma_{v,i}$ refers to the velocity dispersion. The anisotropy of the velocity dispersion has been observed by the Sloan Digital Sky Survey and Gaia. Approximately we have the relation $\sigma_{v,r} \simeq 2\sigma_{v,\theta/\phi}$ for stars with high metallicity, which may originate from a major merger event of a satellite galaxy between 8 and 11 Gyr ago (V. Belokurov et al. 2018). For qualitative discussions, we assume the uncertainty $\sigma_v \simeq 100$ km s$^{-1}$ $\simeq 1.01 \times 10^{-4}$ pc yr$^{-1}$ for all stars on both directions on the sky sphere. At a typical distance of 1 kpc,[10] the angular deflection observed over 10 yr reaches $\simeq 1.01 \times 10^{-6}$ rad, which significantly exceeds the single-exposure resolution $\sigma_{ss} \simeq 100\,\mu$as $= 4.85 \times 10^{-10}$ rad of Gaia for a single star. It then becomes necessary to subtract the background proper motion from the data before searching for the GW or DPDM.

We now turn our attention to the accelerations affecting stellar and the Earth's motion. Let us consider stars in two categories: isolated stars and the ones in binary or higher-order systems. For isolated stars, their velocities, in general, change over time. Hence, we should also estimate their accelerations, which mainly include contributions from two aspects:

1. *The constant accelerations of stars.* The density gradient in the milky Way could induce constant accelerations for stars. Unlike their proper motion, the constant accelerations of stars are predictable due to the galactic mass profile, indicating the uncertainty $\sigma_a$ should be much smaller than the center value of the star's acceleration, defined as $\boldsymbol{a}_0$. Typical stars in the Milky Way experience an acceleration of $|\boldsymbol{a}_0| \sim 10^{-10}$ m s$^{-2}$ (H. Silverwood & R. Easther 2019), which leads to a displacement of $|\boldsymbol{a}_0|\Delta t^2/2 \simeq 1.6 \times 10^{-10}$ pc over the 10 yr observation. For a star located 1 kpc away from us, the corresponding angular deflection is about 0.03 $\mu$as, significantly below the detection threshold.

---

[10] The peak distribution of distances between the stars and us observed by Gaia is $1 \sim 2$ kpc (A. Vallenari et al. 2023).
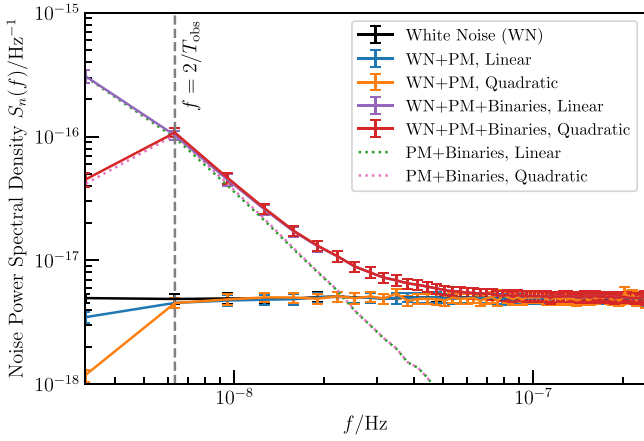
**Figure 1.** The average PSDs of the injected white noise (WN), proper motion (PM), and stellar binary motion, along with the associated error bars for each bin, obtained from $10^4$ simulations. For clarity, the error bars have been magnified by a factor of 3 to improve visibility. The green and pink dashed lines correspond to the cases with WN removed. The vertical dashed line refers to $f = 2/T_{\rm obs}$, with $T_{\rm obs} = 10$ yr being Gaia's observation period. The input Gaia operational parameters align with the discussion in Section 4.

2. *The constant acceleration of the solar system barycenter (SSB).* Like other stellar systems, the velocity of our solar system is not precisely constant. Instead, it follows a curved orbit in the Galaxy. For the observer, the nonzero acceleration of the SSB gives rise to the aberration effect, which can be considered as extra (spurious) proper motion superimposed on stars (S. M. Kopeikin & V. V. Makarov 2006; S. Klioner et al. 2021):

$$\frac{d\delta\boldsymbol{n}}{dt} = \boldsymbol{a}_{\rm SSB} - (\boldsymbol{a}_{\rm SSB} \cdot \boldsymbol{n})\boldsymbol{n}, \qquad (2)$$

where $\delta\boldsymbol{n}$ denotes the displacement in the apparent stellar position due to aberration and $\boldsymbol{a}_{\rm SSB}$ is the acceleration of the SSB. The estimated value of $\boldsymbol{a}_{\rm SSB}$ is $2.32 \times 10^{-10}$ m s$^{-2}$, corresponding to a proper-motion amplitude of 5.05 $\mu$as yr$^{-1}$ (S. Klioner et al. 2021). From Equation (2), we realize that the displacement $\delta\boldsymbol{n}$ is linear in time, as the aberration effect should be proportional to the velocity of the observer. Therefore, although the proper motion caused by $\boldsymbol{a}_{\rm SSB}$ is larger than Gaia's resolution, it can be subtracted by a function that is linearly dependent on time.

In short, the background motion of the apparent stellar locations is governed by the proper motion of stars, which can be significantly greater than the resolution of Gaia. The acceleration of stars is very minor and thus plays a negligible role. Moreover, the acceleration of the SSB yields spurious proper motion, which can be subtracted by a linear function in time. The above backgrounds can be eliminated through a linear subtraction scheme.

Next, we investigate the significant background motion from unresolved binary or higher-order systems in the Galaxy. In the practical numerical calculation, we employ a data compression technique akin to the one described in C. J. Moore et al. (2017) and S. A. Klioner (2018), since the vast number of objects ($\sim 10^9$) in the full data set of Gaia severely slows down the process of numerical simulation. Specifically, we compress the data of $10^5$ stars in the same sky area into one virtual star. For each star, the probability of being part of a binary or high-order system and having specific orbital parameters is statistically independent of the status of the other stars. After data compression, the astrometric data of $10^5$ stars in each sky area are added together. The background motion of individual stars in binary or higher-order systems manifests as a time-dependent noise of the compressed virtual star.

A survey of nearby ($<250$ pc) stellar objects finds $\sim 55\%$ of solar-type stars are isolated, while the remaining $\sim 45\%$ of stars are in binary or higher-order systems (D. Raghavan et al. 2010). Here, we consider a binary system consisting of two objects with masses $m_1$ and $m_2$, for simplicity. Following Kepler's law, the orbital period $P_b$ has the following relation with the semimajor axis $a_b$:

$$a_b = \left[\frac{Gm_1(1 + q)P_b^2}{(2\pi)^2}\right]^{1/3}, \qquad (3)$$

where $G$ is the gravitational constant and $q = m_2/m_1 < 1$. If both stars are observed by Gaia, the net contribution from the binary to the displacement of the stars will approximate to

$$r_{\rm net} \simeq a_b(1 + e_b)\frac{1 - q}{1 + q}, \qquad (4)$$

where $e_b$ is the orbit eccentricity. Then the net contribution will be fully canceled if $q = 1$.

For the $q < 1$ case, we illustrate it by considering an $e_b = 0$ binary composed of two stars with total mass $M = m_1 + m_2$. The net amplitude of the observed angular deflection in one direction is

$$A_b = \frac{r_{\rm net}\lambda(\iota_b, \psi_b)}{\sqrt{2}D_b} = 6.10 \times 10^{-9} \text{ rad}\left(\frac{1 - q}{1 + q}\right)\frac{\lambda(\iota_b, \psi_b)}{\sqrt{2}}$$

$$\times \left[\frac{P_b}{\text{year}}\right]^{2/3}\left[\frac{D_b}{1 \text{ kpc}}\right]^{-1}\left[\frac{M}{2M_\odot}\right]^{1/3}, \qquad (5)$$

where $D_b$ is the distance between the observer and the binary barycenter and $M_\odot$ denotes the solar mass. Also, $\lambda(\iota_b, \psi_b) = \cos\iota_b \sin\psi_b + \cos\psi_b$, with $\iota_b$ and $\psi_b$ being the inclination angle and the polarization angle of the stellar binary plane, respectively. Equation (5) indicates that binaries with $P_b \gtrsim 1$ yr and $D_b \sim 1$ kpc may be resolved by Gaia. According to D. Raghavan et al. (2010) and P. Simonetti et al. (2020), the period distribution approximately follows the log-normal distribution:

$$P(\log_{10} P_b/\text{day}) \simeq \frac{1}{2.28\sqrt{2\pi}}e^{-\frac{(\log_{10} P_b/\text{day} - 5.03)^2}{2 \times 2.28^2}}, \qquad (6)$$

which centers around a period of 293.6 yr. About 20% of stellar binaries have orbital periods from 24 days to 10 yr, which would induce an irreducible background for the 10 yr observation of the Gaia mission.

We calculate the power spectral density (PSD) originating from binary stars $S_{\rm bin}(f)$ by implementing a Monte Carlo simulation, where we assume 45% of stars are in binaries. We use Equation (5) with $D_b = 1$ kpc, while the orbital period is drawn from Equation (6). Furthermore, $\cos\iota_b$, $\psi_b$, and $q$ are treated as free parameters, randomly selected from uniform distributions within the intervals of $[-1, 1)$, $[0, 2\pi)$, and $[0.1, 1)$, respectively. In each simulation, we generate astrometric data for $10^5$ stars, which are then compressed into one virtual star. We calculate the PSD of the astrometric data of the virtual

star. The final $S_{\rm bin}(f)$ is obtained by averaging the PSD over all simulations. The total noise PSD $S_n(f)$ is the combination of $S_{\rm bin}(f)$ and that from the instrumental noise $S_w(f)$, namely

$$S_n(f) = S_w(f) + S_{\rm bin}(f). \qquad (7)$$

We present the average noise PSD in Figure 1, together with the error bars of each bin. The uncertainties of the PSDs estimated from the simulation are around $10^{-19}$ Hz$^{-1}$. In the absence of noise from stellar binaries, the linear/quadratic subtraction approach effectively reduces the noise from stellar proper motion, reproducing the PSD of pure white noise above $2/T_{\rm obs} \sim 6 \times 10^{-9}$ Hz. Nevertheless, the inclusion of binaries indeed introduces significant noise when $f \lesssim 10^{-7}$ Hz, corresponding to $P_b \gtrsim 24$ days. This noise grows as $P_b$ increases, coinciding with the behavior manifested by Equation (5). Furthermore, there are clear breaks in the PSDs at $f = 2/T_{\rm obs}$, because the observed angular deflection of isolated stars or binary systems no longer exhibits periodic oscillations during the duration of Gaia's observations if $f \lesssim 2/T_{\rm obs}$, and consequently two subtraction schemes will reduce the time-dependent noise in the low-frequency region. The quadratic subtraction removes both the linear and quadratic components of the noise, resulting in lower noise PSDs compared to the linear subtraction. However, the quadratic subtraction also leads to more reductions in our signal at low frequencies, and we will see that linear subtraction achieves a better signal-to-noise ratio eventually.

## 3. Astrometric Deflections Induced by GW and DPDM

### 3.1. GWs from Binary Systems

To begin with, we revisit the formula for light deflection induced by GWs (T. Pyne et al. 1996; L. G. Book & E. E. Flanagan 2011). The presence of GWs triggers metric perturbations, which lead to the slight deflection of light traveling from a star to the Earth, ultimately resulting in the apparent displacement of stellar positions. By repeatedly measuring the apparent positions of a large number of stars across the sky, Gaia might be capable of capturing such deflection and thus extracting the characteristic patterns of GWs.

The variation in the line-of-sight direction $n^i$ due to GWs can be expressed as (T. Pyne et al. 1996; L. G. Book & E. E. Flanagan 2011)

$$\delta n_{\rm GW}^i \simeq \frac{n^i - p^i}{2(1 - \boldsymbol{n} \cdot \boldsymbol{p})} h_{jk}^{\rm GW}({\rm E}) n^j n^k - \frac{1}{2} h_{ij}^{\rm GW}({\rm E}) n^j, \qquad (8)$$

where the unit vector $\boldsymbol{p}$ described by two rotational angles $\theta_p$ and $\varphi_p$ represents the propagated direction, with $p^i$ being its components, and $h_{ij}^{\rm GW}({\rm E})$ refers to the metric perturbation calculated at the Earth. The metric perturbation $h_{ij}^{\rm GW}$ caused by monochromatic GWs with frequency $f_{\rm GW}$ reads

$$h_{ij}^{\rm GW}(t, \boldsymbol{x}) = {\rm Re}\,[\mathcal{H}_{ij}^{\rm GW} e^{2\pi i f_{\rm GW}(t - \boldsymbol{p} \cdot \boldsymbol{x})}], \qquad (9)$$

with $\mathcal{H}_{ij}^{\rm GW}$ denoting the amplitude tensor. The GW possesses two polarization directions, and thus $\mathcal{H}_{ij}^{\rm GW}$ can be written in the following form:

$$\mathcal{H}_{ij}^{\rm GW} = h_+^{\rm GW} \epsilon_{ij}^+(\boldsymbol{p}, \psi) e^{i\phi_+} + h_\times^{\rm GW} \epsilon_{ij}^\times(\boldsymbol{p}, \psi) e^{i\phi_\times}, \qquad (10)$$

where $\epsilon_{ij}^+$ and $\epsilon_{ij}^\times$ are two polarization tensors depending on $\boldsymbol{p}$ and the GW polarization angle $\psi$ (Z. Arzoumanian et al. 2023), $h_+^{\rm GW}$ and $h_\times^{\rm GW}$ are their amplitudes, and $\phi_+$ and $\phi_\times$ are two corresponding phases. We consider the monochromatic GW radiated from a binary system with a circular orbit, the amplitudes $h_+^{\rm GW}$ and $h_\times^{\rm GW}$ of which can be respectively expressed as

$$h_+^{\rm GW} = h_0^{\rm GW} \frac{1 + \cos^2 \iota}{2}, \ h_\times^{\rm GW} = h_0^{\rm GW} \cos \iota, \qquad (11)$$

where $h_0^{\rm GW}$ is nearly a constant, depending on the chirp mass, the angular orbital frequency, and the luminosity distance to the source, and $\iota$ is the inclination angle of the binary. Finally, for the circular orbit, the relation $\varphi_+ - \varphi_\times = \pi/2$ should be satisfied.

We omit the "star term" in Equation (8). According to C. J. Moore et al. (2017), the ratio between the "star term" and the "Earth term" equals the ratio between the wavelength of the GW and the distance to the source. For a GW frequency of $>10^{-10}$ Hz, the wavelength is $<100$ pc, making the "star term" significantly smaller than the "Earth term," assuming that the star is located 1 kpc away from us. Moreover, the "star terms" from different sources are uncorrelated, resembling a kind of random noise, causing the "star terms" to be further suppressed after data compression, compared to the "Earth term" that is consistently coherent.

### 3.2. DPDM with Purely Gravitational Interactions

Analogous to GWs, dark photon fields can also induce metric fluctuations via gravitational effects (A. E. Nelson & J. Scholtz 2011; A. Khmelnitsky & V. Rubakov 2014; K. Nomura et al. 2020). In this subsection, we derive the angular deflection of light emitted from the star as it passes through DPDM with purely gravitational interactions due to metric perturbations. We should mention that DPDM with a mass below $10^{-22}$ eV is subject to severe constraints from, e.g., the integrated Sachs–Wolfe effect on cosmic microwave background anisotropies ($\gtrsim 10^{-24}$ eV; R. Hlozek et al. 2015), the stellar kinematics of dwarf spheroidal galaxies (a few times $10^{-23}$ eV; A. X. González-Morales et al. 2017; E. Kendall & R. Easther 2020), and the Ly$\alpha$ forest ($\gtrsim 10^{-21}$ eV; E. Armengaud et al. 2017; L. Hui et al. 2017). The lower bound on ultralight dark matter mass is still under debate; here we treat the local dark matter density $\rho_{\rm DM}$ as a free parameter.

We first describe the DPDM model. The dark photon field is expressed as

$$\boldsymbol{A}(t, \boldsymbol{x}) \simeq A_0(\boldsymbol{x}) {\rm Re}\,[\boldsymbol{q}(\boldsymbol{x}) \exp(im_A t)], \qquad (12)$$

where the polarization vector $\boldsymbol{q}(\boldsymbol{x}) = (\cos \theta_q \cos \varphi_q e^{i\phi_1}, \cos \theta_q \sin \varphi_q e^{i\phi_2}, \sin \theta_q e^{i\phi_3})^T$ is parameterized by two polarization angles $\theta_q$ and $\varphi_q$ and three phases $\phi_1$, $\phi_2$, and $\phi_3$, all of which are in general certain functions of $\boldsymbol{x}$. Under the synchronous gauge, the metric perturbation has the following form:

$$h_{ij}^{\rm DP}(t, \boldsymbol{x}) \simeq {\rm Re}\,[\mathcal{H}_{ij}^{\rm DP}(\boldsymbol{x}) e^{2im_A t}], \qquad (13)$$

where

$$\mathcal{H}_{ij}^{\rm DP}(\boldsymbol{x}) = -h_0^{\rm DP}\left[q_i(\boldsymbol{x}) q_j(\boldsymbol{x}) - \frac{\boldsymbol{q}(\boldsymbol{x}) \cdot \boldsymbol{q}(\boldsymbol{x}) \delta_{ij}}{4}\right]. \qquad (14)$$

The signal amplitude can be written as $h_0^{\mathrm{DP}} = 4\pi G A_0^2(\boldsymbol{x})$, with $A_0(\boldsymbol{x})$ being the amplitude of the dark photon field. The amplitude of DPDM is

$$A_0(\boldsymbol{x}) = \frac{\sqrt{2\rho_{\mathrm{DM}}(\boldsymbol{x})}}{m_A}, \qquad (15)$$

where $\rho_{\mathrm{DM}}(\boldsymbol{x})$ is the energy density of the DPDM. A detailed derivation of Equation (13) can be found in Appendix A. As a result, we can estimate the signal amplitude:

$$h_0^{\mathrm{DP}} = 5.2 \times 10^{-15}\left(\frac{\rho_{\mathrm{DM}}}{0.4\,\mathrm{GeV\,cm}^{-3}}\right)\left(\frac{10^{-23}\,\mathrm{eV}}{m_A}\right)^2. \qquad (16)$$

It is known that the metric perturbation $h_{ij}^{\mathrm{DP}}$ given in Equation (13) yields a delay of the arrival time of the pulsar light, which can be probed by PTAs (K. Nomura et al. 2020; Y.-M. Wu et al. 2022; X. Xue et al. 2022; Z.-Q. Xia et al. 2023). Here, we show that the same metric perturbation could also lead to the deflection of the star's proper position, namely

$$\delta n_{\mathrm{DP}}^i \simeq -\frac{(\delta^{ik} - n^i n^k)}{2} n^j h_{jk}^{\mathrm{DP}}(\mathrm{E}) + \mathcal{O}(v_{\mathrm{vir}}), \qquad (17)$$

where we have omitted terms relying on the virial velocity $v_{\mathrm{vir}}$. The complete gauge-invariant expressions of $\delta n_{\mathrm{DP}}^i$ can be found in Appendix B. The perturbation $h_{jk}^{\mathrm{DP}}(\mathrm{E})$ is again calculated at the Earth and we ignore all the "star terms." In Appendices B.1, B.2, and B.3, we demonstrate that this approximation is valid as long as $m_A \geqslant 10^{-24}\,\mathrm{eV}$.

### 3.3. DPDM with Additional Gauge Couplings

DPDM can also interact with ordinary matter if it is associated with $U(1)_B$ or $U(1)_{B-L}$ gauge symmetry. As a consequence, any baryonic matter could experience an oscillating force due to the DPDM background, leading to an acceleration $\boldsymbol{a}$ given by (A. Pierce et al. 2018)

$$\boldsymbol{a}(t, \boldsymbol{x}) \simeq \epsilon e \frac{q_{\mathrm{obj}}}{m_{\mathrm{obj}}} \frac{\partial}{\partial t} \boldsymbol{A}(t, \boldsymbol{x}), \qquad (18)$$

where $\epsilon$ is the coupling constant of the dark photon, $e$ denotes the electromagnetic coupling constant, $q_{\mathrm{obj}}$ refers to the $B$ or $B-L$ charge the object carries, and $m_{\mathrm{obj}}$ is the mass of the test object.

The above acceleration leads to a velocity variation of the object

$$\delta \boldsymbol{v}(t, \boldsymbol{x}) = \epsilon e \frac{q_{\mathrm{obj}}}{m_{\mathrm{obj}}} \boldsymbol{A}(t, \boldsymbol{x}), \qquad (19)$$

which can cause aberrations of the stellar proper motion due to the moving observer (H.-K. Guo et al. 2019). The resulting apparent angular deflection can be expressed as

$$\delta \boldsymbol{n}_{B/B-L}(t, \boldsymbol{n}) = \delta \boldsymbol{v}(t, \boldsymbol{x}_{\mathrm{E}}) - (\delta \boldsymbol{v}(t, \boldsymbol{x}_{\mathrm{E}}) \cdot \boldsymbol{n})\boldsymbol{n}, \qquad (20)$$

where $\boldsymbol{x}_{\mathrm{E}}$ is the coordinate of the observer and $\boldsymbol{n}$ is the sky location of the star. Moreover, the dark photon field can also directly lead to stellar motion, with an amplitude approximated by $\delta \boldsymbol{n}_{B/B-L}^s \lesssim |\delta \boldsymbol{v}| \cdot t/D$ (with $D$ being the distance between the star and the Earth). However, for the typical observation time ($\sim 1\,\mathrm{yr}$) and distance $D \gtrsim 1\,\mathrm{kpc}$, $\delta \boldsymbol{n}_{B/B-L}^s \sim 3 \times 10^{-4} \delta \boldsymbol{n}_{B/B-L}$ is rather tiny and will not be taken into consideration (H.-K. Guo et al. 2019).

## 4. Sensitivity of GW and DPDM Searches with Gaia

In this section, we estimate the sensitivity of Gaia-like astrometry for GW- and DPDM-induced signals. We consider both Gaia and its next-generation upgrade ("XG-Gaia"), where we anticipate that XG-Gaia will achieve $\mu$as angular resolution while maintaining the same number of observed stars as Gaia does (A. Vallenari 2018). The operational parameters of these missions are set as follows:

$$\begin{aligned} \text{Gaia:} \quad & \sigma_{\mathrm{ss}} = 100\,\mu\mathrm{as}, \ \Delta t = 24\,\mathrm{days}, \\ & T_{\mathrm{obs}} = 10\,\mathrm{yr}, N = 1 \times 10^9; \\ \text{XG-Gaia:} \quad & \sigma_{\mathrm{ss}} = 1\,\mu\mathrm{as}, \ \Delta t = 24\,\mathrm{days}, \\ & T_{\mathrm{obs}} = 20\,\mathrm{yr}, N = 1 \times 10^9, \end{aligned}$$

where $\sigma_{\mathrm{ss}}$ is the noise from a single exposure,[11] $\Delta t$ is the observational cadence, $T_{\mathrm{obs}}$ is the total observation time, and $N$ is the total number of stars considered in the analysis.

As previously mentioned, we compress the data of $10^5$ stars in the same sky area by randomly generating $\widetilde{N} = 10^4$ virtual stars uniformly distributed across the sky. Consequently, the instrument error for the measurement on each virtual star is rescaled to $\tilde{\sigma} = \sigma_{\mathrm{ss}}/\sqrt{10^9/10^4}$. To estimate the sensitivity in detecting GWs and DPDM with Gaia-like experiments, we construct a mock data set by injecting a specific GW or DPDM signal into the virtual stars. At the end of Sections 3.1, 3.2, and 3.3, we demonstrated that the signals we considered are consistently dominated by the "Earth term" for $f_{\mathrm{GW}} > 10^{-10}\,\mathrm{Hz}$ or $m_A > 10^{-24}\,\mathrm{eV}$. Therefore, the astrometric effects on the stars in one area, caused by GWs or DPDM, can be approximated to the global effect on the virtual stars within that area.

In addition to the signal component, in Section 2 we have established that the background motion due to stellar proper motion and the acceleration of the SSB are effectively removed by linear subtraction. The constant acceleration resulting from the galaxy's mass distribution is sufficiently small, thus can be safely ignored. Since linear subtraction is consistently applied to the astrometric data of virtual stars, background motion is not injected into the analysis. To address the time-dependent noise caused by stellar binaries, we adopt two different strategies for Gaia and XG-Gaia:

1. For Gaia, we assume that all stellar binaries are unresolvable. Thus, we use the PSD $S_{\mathrm{bin}}(f)$ calculated in Section 2, as shown in Figure 1.
2. For XG-Gaia, with $\sigma_{\mathrm{ss}} = 1\,\mu\mathrm{as}$, binaries with net amplitudes $A_b \lesssim \sigma_{\mathrm{ss}}$ constitute only 0.01%, according to Equations (5) and (6). Therefore, we assume that almost all binaries have been resolved and removed from the data. Consequently, only single stars ($\sim 55\%$ of the total stars) are used for numerical simulation and $S_{\mathrm{bin}}(f) = 0$.

We construct $\chi^2$-functions for both the signal hypothesis and null hypothesis in the frequency domain, namely:

$$\chi_s^2 = \frac{2}{T_{\mathrm{obs}}} \sum_{I,K} \frac{|\widetilde{\boldsymbol{d}}_I(f_K) - \widetilde{s}_I(\Phi; f_K)|^2}{S_n(f_K)}, \qquad (21)$$

---

[11] The uncertainties on the proper-motion parameters depend on the stellar magnitudes $G$. It is expected that the final uncertainty $\sigma_{\mathrm{ss}} \simeq 100\,\mu\mathrm{as}$ for stars with $G \simeq 20$ in Gaia DR5 (A. Vallenari et al. 2023). As these stars constitute the vast majority of the Gaia data set, we will use $\sigma_{\mathrm{ss}} = 100\,\mu\mathrm{as}$ for all stars later on.
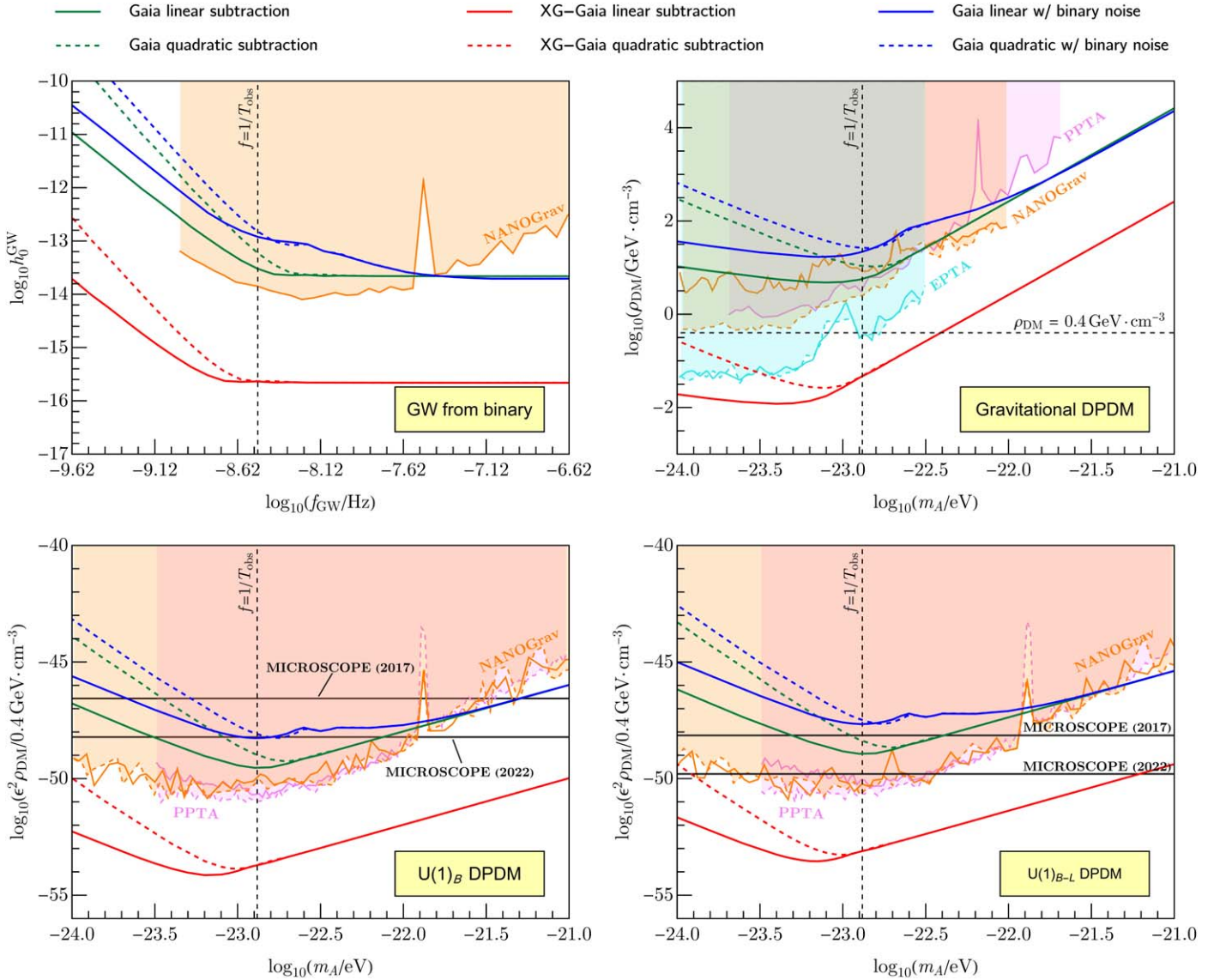
**Figure 2.** The 95% exclusion limits from Gaia (green lines) and XG-Gaia (red lines) on the GW strain $h_0^{\rm GW}$ from a binary system, the energy density $\rho_{\rm DM}$ of the DPDM with purely gravitational interactions, and the coupling constant $\epsilon$ of $U(1)_B/U(1)_{B-L}$ DPDM, respectively. Model parameters regarding all the angles have been integrated out. The solid lines represent the bounds with linear subtraction, while the dashed lines correspond to quadratic subtraction. We also use the blue lines to denote the results including the time-dependent noise from unresolved binary systems. For comparison, the constraints from NANOGrav 15 yr (A. Afzal et al. 2023; G. Agazie et al. 2023b), EPTA DR2 (C. Smarra et al. 2023), and PPTA DR2 (Y.-M. Wu et al. 2022; X. Xue et al. 2022) are shown by the orange, cyan, and purple curves, respectively, with the solid (dashed) curves being the (un)correlated constraints. In the top right panel, the black dashed line shows the amount of local dark matter density near the Earth as a reference. In the bottom two panels, the horizontal solid lines are the limits from the MICROSCOPE WEP experiment (P. Touboul et al. 2017, 2022; P. Fayet 2018, 2019; D. W. P. Amaral et al. 2024). In addition, the vertical dashed line in each plot refers to the reference frequency $f = 1/T_{\rm obs}$, with $T_{\rm obs} = 10$ yr being Gaia's observation period.

and

$$\chi_n^2 = \frac{2}{T_{\rm obs}} \sum_{I,K} \frac{|\tilde{d}_I(f_K)|^2}{S_n(f_K)}, \qquad (22)$$

where $\tilde{d}_I$ is the astrometry data of the virtual star $I$ after linear or quadratic subtraction, $\tilde{s}_I(\Phi; f_K)$ represents the model predictions for a given set of parameters $\Phi$ after the same subtraction strategy, and $S_n(f)$ is defined in Equation (7) with $S_w(f) = \tilde{\sigma}\Delta t$. Note that both $\tilde{d}_I$ and $\tilde{s}_I$ are the quantities after Fourier transforms, and we sum over $I$ and $K$, which correspond to the number of virtual stars and that of bins in

the PSD, respectively. The difference between the signal hypothesis and null hypothesis, i.e., $\Delta \chi^2 = \chi_s^2 - \chi_n^2$, becomes an indicator for measuring the significance of the signal.

The free parameters in $\Phi$ for (A) GWs from binary systems, (B) DPDM with purely gravitational interactions, and (C) DPDM with $U(1)_B$ or $U(1)_{B-L}$ gauge symmetry are respectively:

(A):  $\{f_{\rm GW}, h_0^{\rm GW}, \theta_p, \varphi_p, \iota, \psi, \phi_+\}$;

(B):  $\{m_A, \hat{\rho}_{\rm DM}, \theta_q, \varphi_q, \phi_1, \phi_2, \phi_3\}$;

(C):  $\{m_A, \epsilon^2\hat{\rho}_{\rm DM}, \theta_q, \varphi_q, \phi_1, \phi_2, \phi_3\}$,

where

$$\hat{\rho}_{DM} \equiv \frac{\rho_{DM}}{0.4\ \text{GeV cm}^{-3}}. \quad (23)$$

We fix the values of $f_{GW}$ and $m_A$ and scan the other model parameters in their individual parameter space in each case. The 95% exclusion limits on $h_0^{GW}$, $\rho_{DM}$, and $\epsilon$ after integrating out all angular parameters are shown in Figure 2. Some remarks are in order. First, the frequency $f = 2/T_{obs}$ approximately marks where the sensitivity curves show significant changes. In the high-frequency range ($f \gtrsim 2/T_{obs}$), the limits obtained using two different subtraction methods are indistinguishable, as expected, whereas linear subtraction offers better sensitivity in the low-frequency range compared to quadratic subtraction. In particular, the 95% exclusion limits are enhanced by more than 1 order of magnitude at $f_{GW} \lesssim 6 \times 10^{-10}$ Hz for GWs or at $m_A \lesssim 3 \times 10^{-24}$ eV for DPDM. Second, the impact of time-dependent noise from unresolved binary systems significantly decreases the sensitivity by up to an order of magnitude. Hence, the inclusion of such noise is important in our analysis. In addition, this decrease is more severe in the linear subtraction scheme than in the quadratic subtraction, as we explained in Section 2. Last, XG-Gaia will possess extended observation duration and improved precision. It will also have enhanced resolution capabilities for binary systems, which are crucial for suppressing the noise from unresolved binaries. As a result, the sensitivity of XG-Gaia to detecting GWs and DPDM is expected to increase by more than 3 orders of magnitude.

## 5. Conclusion

Astrometric measurements offer a new approach to detecting signals such as GWs and DPDM in the nanohertz frequency range. Typically, periodic signals with frequencies below $1/T_{obs}$ are easily mistaken for background noise or systematic uncertainties. Known background sources include (1) the proper motion of stars, (2) stellar acceleration due to the Milky Way's mass distribution, (3) acceleration from companion stars in binary systems, and (4) the Earth's acceleration. In Section 2, we demonstrate that a linear subtraction method is sufficient to remove all these effects. Compared to the commonly used quadratic subtraction, linear subtraction significantly enhances detection sensitivity in the low-frequency range.

However, other factors, such as telescope movement, changes in satellite orientation, and unknown systematics, are not investigated here. We project detection prospects in this study, assuming all these systematics are properly subtracted. We emphasize that future detection claims will require more detailed studies of these systematics. Furthermore, this work does not explore the angular patterns induced by GWs and DPDM, which may be crucial for distinguishing between systematics and genuine signals.

Astrometric data can also be correlated with the current existing PTA data, allowing for a more concrete validation of the correlation pattern induced by GWs or dark matter and a more sensitive probe of the macroscopic polarizations of the GWs (W. Qin et al. 2019, 2021; M. Çalışkan et al. 2024). Compared to PTAs, future astrometric surveys like Roman (Y. Wang et al. 2021, 2022) will be able to probe microhertz

GWs or beyond and ultralight bosons with higher masses, allowing for cross-correlation with other proposed measurements in the same frequency range, such as binary resonance (D. Blas & A. C. Jenkins 2022a, 2022b) and Doppler tracking (L. Zwick et al. 2024), potentially closing the gap between the PTA and LISA frequency ranges.

**Note added:** During the preparation of this paper, we became aware of the recent works by H. Kim (2024) and J. A. Dror & S. Verner (2024), which consider the astrometric effect of the ultralight scalar dark matter. Our work focuses on the detection of the ultralight vector dark matter and continuous GWs, which is distinctive from their themes.

## Appendix A
## Metric Perturbation Induced by DPDM

Consider a general metric perturbation $h_{\mu\nu}$; the equation of motion can be written as (S. M. Carroll 2019)

$$\Box h_{\mu\nu} - \partial^\alpha \partial_\nu h_{\mu\alpha} - \partial^\alpha \partial_\mu h_{\nu\alpha} + \partial_\mu \partial_\nu h$$
$$+ \eta_{\mu\nu}(\partial^\alpha \partial^\beta h_{\alpha\beta} - \Box h) = -16\pi G T_{\mu\nu}, \quad (A1)$$

where $h \equiv h_{\mu\nu}\eta^{\mu\nu}$ and $\Box \equiv \partial^\mu \partial_\mu$. We work in the Minkowski background $\eta_{\mu\nu} = \text{diag}(-1, 1, 1, 1)$. Under the gauge fixing condition $h_{0\mu} = 0$, the Einstein equations become

$$-16\pi G T_{00} = \partial_0^2 h - (\partial_k \partial_l h_{kl} - \Box\, h), \quad (A2)$$

$$-16\pi G T_{0i} = -\partial_k \partial_0 h_{ik} + \partial_i \partial_0 h, \quad (A3)$$

$$-16\pi G T_{ij} = \Box h_{ij} - \partial_k \partial_i h_{jk} - \partial_k \partial_j h_{ik}$$
$$+ \partial_i \partial_j h + \delta_{ij} \partial_k \partial_l h_{kl} - \delta_{ij} \Box\, h. \quad (A4)$$

From Equation (A4), we find

$$-2\,\Box\, h + \nabla^2 h + \partial_l \partial_j h_{jl} = -16\pi G T_{kk}. \quad (A5)$$

It is also convenient to derive

$$-16\pi G\left(T_{ij} - \frac{\delta_{ij}}{2}T_{kk}\right) = \Box\, h_{ij} - \partial_k\partial_i h_{jk} - \partial_k\partial_j h_{ik}$$
$$+ \partial_i\partial_j h + \frac{1}{2}\delta_{ij}\partial_k\partial_l h_{kl} - \frac{1}{2}\delta_{ij}\nabla^2 h. \quad (A6)$$

Next we calculate the stress–energy tensor induced by the DPDM. The virial velocity of our galaxy is $v_{\rm vir} \simeq \mathcal{O}(10^{-3})$, so for ultralight DPDM with mass $m_A \sim 10^{-23}$ eV, the de Broglie wavelength is $\lambda_{\rm dB} \sim 4\,{\rm kpc}(10^{-23}\,{\rm eV}/m_A)(10^{-3}/v_{\rm vir})$, which is of the same order as the galactic size. The coherence time is $t_c \sim 1/(m_A v_{\rm vir}^2) = 2\,{\rm Myr}(10^{-23}\,{\rm eV}/m_A)(10^{-3}/v_{\rm vir})^2$. Since we are considering DPDM within a coherent time, we can write down the spatial component of the dark photon field as

$$\boldsymbol{A}(t, \boldsymbol{x}) = A_0(\boldsymbol{x})\,{\rm Re}\,[\boldsymbol{q}(\boldsymbol{x})e^{iEt}], \quad (A7)$$

where $E = m_A\sqrt{1 + \mathcal{O}(v_{\rm vir}^2)}$ and $\boldsymbol{q}(\boldsymbol{x})$ is a complex vector that characterizes the polarization of the dark photon field, normalized as $|\boldsymbol{q}| = 1$. The spatial derivative of $A(\boldsymbol{x})$ and $\boldsymbol{q}(\boldsymbol{x})$ is suppressed by virial velocity $v_{\rm vir}$. Using the equation of motion $\partial_\mu A^\mu = 0$, we find that the scalar potential of the dark photon field $A^t$ is suppressed by $v_{\rm vir}$:

$$A^t = \mathcal{O}(v_{\rm vir}). \quad (A8)$$

The stress–energy tensor of the vector field reads

$$T_{\mu\nu}(t, \boldsymbol{x}) = \eta_{\mu\nu}\left(-\frac{1}{4}F_{\rho\sigma}F^{\rho\sigma} - \frac{1}{2}m^2 A^\rho A_\rho\right)$$
$$+ \eta^{\rho\sigma}F_{\mu\sigma}F_{\nu\rho} + m^2 A_\mu A_\nu. \quad (A9)$$

We find that at the zeroth order of $v_{\rm vir}$, the relevant components of the stress–energy tensor are

$$T_{00}^{(0)} = \rho(\boldsymbol{x}), \qquad T_{0k}^{(0)} = 0,$$
$$T_{kk}^{(0)} = -\rho(\boldsymbol{x})\,{\rm Re}[\boldsymbol{q}(\boldsymbol{x})\cdot\boldsymbol{q}(\boldsymbol{x})\,e^{2im_A t}],$$
$$T_{ij}^{(0)} - \frac{\delta_{ij}}{2}T_{kk} = 2\rho(\boldsymbol{x})\,{\rm Re}$$
$$\times \left\{\left[q_i(\boldsymbol{x})q_j(\boldsymbol{x}) - \frac{\boldsymbol{q}(\boldsymbol{x})\cdot\boldsymbol{q}(\boldsymbol{x})\delta_{ij}}{4}\right]e^{2im_A t}\right\}, \quad (A10)$$

where for simplicity we define $\rho(\boldsymbol{x}) \equiv m_A^2 A_0^2(\boldsymbol{x})/2$. By combining Equations (A2) and (A5), we can eliminate $\partial_l\partial_k h_{kl}$ and get (hereafter, we add the superscript "DP" for quantities associated with the DPDM)

$$\partial_0^2 h^{\rm DP} = -8\pi G(T_{00} + T_{kk}) = -8\pi G\rho(\boldsymbol{x})$$
$$\times \{1 - {\rm Re}\,[\boldsymbol{q}(\boldsymbol{x})\cdot\boldsymbol{q}(\boldsymbol{x})\,e^{2im_A t}]\}. \quad (A11)$$

Integrating Equation (A11), we find that the trace $h$ contains at least an oscillating component:

$$h^{\rm DP}(\boldsymbol{x}) = -\frac{8\pi G\rho(\boldsymbol{x})}{m_A^2}{\rm Re}\left[\frac{\boldsymbol{q}(\boldsymbol{x})\cdot\boldsymbol{q}(\boldsymbol{x})}{4}\,e^{2im_A t}\right], \quad (A12)$$

which suggests that $h_{ij}$ also has an oscillating part and a static part:

$$h_{ij}^{\rm DP}(t, \boldsymbol{x}) = -h_0^{\rm DP}(\boldsymbol{x})\,{\rm Re}\,[\mathcal{H}_{ij}^{\rm DP}(\boldsymbol{x})\,e^{2im_A t}]. \quad (A13)$$

Combining Equations (A6) and (A10), we obtain

$$-32\pi G\rho(\boldsymbol{x})\,{\rm Re}\left\{\left[q_i(\boldsymbol{x})q_j(\boldsymbol{x}) - \frac{\boldsymbol{q}(\boldsymbol{x})\cdot\boldsymbol{q}(\boldsymbol{x})\delta_{ij}}{4}\right]e^{2im_A t}\right\}$$
$$= \Box\, h_{ij}^{\rm DP} - \partial_k\partial_i h_{jk}^{\rm DP} - \partial_k\partial_j h_{ik}^{\rm DP} + \partial_i\partial_j h^{\rm DP}$$
$$+ \frac{1}{2}\delta_{ij}\partial_k\partial_l h_{kl}^{\rm DP} - \frac{1}{2}\delta_{ij}\nabla^2 h^{\rm DP}, \quad (A14)$$

which is accurate to the zeroth order of $v_{\rm vir}$. We extract the oscillation parts on both sides of Equation (A14), which yields

$$\partial_0^2 {\rm Re}\,[-h_0^{\rm DP}(\boldsymbol{x})\mathcal{H}_{ij}^{\rm DP}(\boldsymbol{x})\,e^{2im_A t}] = 32\pi G\rho(\boldsymbol{x})\,{\rm Re}$$
$$\times \left\{\left[q_i(\boldsymbol{x})q_j(\boldsymbol{x}) - \frac{\boldsymbol{q}(\boldsymbol{x})\cdot\boldsymbol{q}(\boldsymbol{x})\delta_{ij}}{4}\right]e^{2im_A t}\right\}, \quad (A15)$$

where we neglect the terms with spatial derivatives, since they are suppressed by $v_{\rm vir}$. Solving this equation, we get

$$\mathcal{H}_{ij}^{\rm DP}(\boldsymbol{x}) = q_i(\boldsymbol{x})q_j(\boldsymbol{x}) - \frac{\boldsymbol{q}(\boldsymbol{x})\cdot\boldsymbol{q}(\boldsymbol{x})\delta_{ij}}{4} \quad (A16)$$

and

$$h_0^{\rm DP}(\boldsymbol{x}) = \frac{8\pi G\rho(\boldsymbol{x})}{m_A^2}. \quad (A17)$$

## Appendix B
## Gauge Invariance of the Angular Deflection

In this appendix, we calculate the angular deflection of light from stars due to the oscillating metric perturbations. This part follows the discussion in L. G. Book & E. E. Flanagan (2011). In this part, we also prove the gauge invariance of the angular deflection. Consider a general metric perturbation

$$ds^2 = g_{\mu\nu}dx^\mu dx^\nu = (\eta_{\mu\nu} + h_{\mu\nu})dx^\mu dx^\nu, \quad (B1)$$

where we work in the Minkowski background with $\eta_{\mu\nu} = {\rm diag}\{-1, 1, 1, 1\}$. Now consider that a photon travels from the source to the detector, so the angular deflection of light we need to calculate becomes the angular difference of the observed photon momentum compared to the flat-spacetime case. Without metric perturbation, we choose the detector to be at the origin $(0, \boldsymbol{0})$ and the unperturbed photon worldline to be $x_{(0)}^\mu = \omega_0\mathcal{N}^\mu\lambda$, where $\boldsymbol{n}$ is the unit vector of the source, $\omega_0$ is the unperturbed photon frequency, and $\mathcal{N}^\mu = (1, -\boldsymbol{n})$. The unperturbed photon four-momentum is $k_{(0)}^\mu = \omega_0\mathcal{N}^\mu$. Suppose the unperturbed position of the source is $x_s^i(t) = x_s^i$, then the affine parameter of the source is $\lambda_s = -|\boldsymbol{x}_s|/\omega_0$.

We separate the photon worldline into unperturbed parts and the first-order perturbation

$$k^\mu(\lambda) = k_{(0)}^\mu(\lambda) + k_{(1)}^\mu(\lambda) + \mathcal{O}(h^2). \quad (B2)$$

To the first order of $h$, the geodesic equation of the photon is

$$\frac{dk^\rho}{d\lambda} = -\Gamma_{\mu\nu}^\rho k_{(0)}^\mu k_{(0)}^\nu. \quad (B3)$$

We integrate the above expression from $\lambda = 0$ to arbitrary $\lambda$ to obtain $k^\mu(\lambda)$:

$$k^\mu(\lambda) = k^\mu_{(0)} + \kappa^\mu - \int_0^\lambda \Gamma^\rho_{\mu\nu} k^\mu_{(0)} k^\nu_{(0)} d\lambda', \qquad (B4)$$

where $\kappa^\mu$ is the first-order perturbation of the photon four-momentum at $\lambda = 0$. Integrating Equation (B4) yields the trajectory of the photon:

$$x^\mu(\lambda) = \lambda(k^\mu_{(0)} + \kappa^\mu) - \int_0^\lambda \int_0^{\lambda'} \Gamma^\rho_{\mu\nu}(\lambda') k^\mu_{(0)} k^\nu_{(0)} d\lambda' d\lambda' + x^\mu(0), \qquad (B5)$$

where $x^\mu(0)$ is the final position of the photon, which also refers to the position of the detector. Choosing $\lambda = \lambda_s$ in Equation (B5), we are able to solve $\kappa^\mu$:

$$\kappa^\mu = \frac{1}{\lambda_s}\left( x^\mu(\lambda_s) - x^\mu(0) + \int_0^{\lambda_s} \int_0^{\lambda'} \right.$$
$$\left. \times \Gamma^\mu_{\gamma\nu}(\lambda'') k^\gamma_{(0)} k^\nu_{(0)} d\lambda'' d\lambda' \right) - k^\mu_{(0)}. \qquad (B6)$$

To the zeroth order of perturbation, $x^\mu(\lambda_s) - x^\mu(0) = \lambda_s k^\mu_{(0)}$. With the presence of metric perturbation, we cannot assume that the detector and source are static, since the geodesic equations of their spatial trajectories also contain $\mathcal{O}(h)$ perturbations. Therefore, we keep $x^\mu(\lambda_s)$ and $x^\mu(0)$ in the expression of $\kappa^\mu$.

In addition, the null geodesic equation constraint $g_{\mu\nu}(\lambda) k^\mu(\lambda) k^\nu(\lambda) = 0$ provides

$$\kappa_0 = n_i \kappa_i - \frac{1}{2\omega_0} h_{\mu\nu}(0) k^\mu_{(0)} k^\nu_{(0)}. \qquad (B7)$$

To calculate the angular deflection the detector observes, we need to project the photon four-momentum into the local proper reference frame of the detector. We define the four-momentum of the detector as $e^\nu_0$ and a set of orthonormal basis vectors as $e^\nu_i$, $i = 1, 2, 3$. We decompose the basis vectors into unperturbed parts and the first-order perturbations

$$e^\nu_\alpha = \delta^\nu_\alpha + \delta e^\nu_\alpha, \quad \alpha = 0, 1, 2, 3. \qquad (B8)$$

The basis vectors of the local proper reference frame satisfy

$$e^\mu_0 \nabla_\mu e^\nu_\alpha = 0. \qquad (B9)$$

Inserting Equation (B8) into Equation (B9), we find

$$\partial_0 \delta e^\nu_\alpha + \Gamma^\nu_{\alpha 0} = 0. \qquad (B10)$$

The orthonormal conditions of $e^\nu_\alpha$ imply

$$g_{\mu\nu} e^\nu_\alpha e^\mu_\beta = \delta_{\alpha\beta}. \qquad (B11)$$

We keep only the first-order terms of Equation (B11), which gives another constraint on $\delta e^\nu_\alpha$:

$$h_{\mu\nu} + \eta_{\mu\gamma} \delta e^\gamma_\nu + \eta_{\nu\gamma} \delta e^\nu_\mu = 0. \qquad (B12)$$

The angular deflection of the dark photon reads

$$\delta n_i = -\frac{g_{\nu\mu}(0) k^\nu(0) e^\mu_i}{\omega_d} - n_i, \qquad (B13)$$

where $\omega_d = -g_{\nu\mu}(0) k^\nu$ is the observed photon frequency. Expanding Equation (B13) to the first order, we obtain

$$\delta n_i = -\frac{1}{\omega_0}(h_{\nu i}(0) k^\nu_{(0)} + \kappa_i + \eta_{\nu\mu} k^\nu_{(0)} \delta e^\mu_i$$
$$- n_i(h_{\nu 0}(0) k^\nu_{(0)} + \eta_{\nu\mu} k^\nu_{(0)} \delta e^\mu_0 + \kappa_0)). \qquad (B14)$$

Plugging Equation (B7) into Equation (B14), we find

$$\delta n_i = -\frac{1}{\omega_0} P_{ij} \kappa_j - h_{\nu i}(0) \mathcal{N}^\nu - \mathcal{N}_\mu \delta e^\mu_i$$
$$+ n_i(h_{\nu 0}(0) \mathcal{N}^\nu + \mathcal{N}_\mu k^\mu_{d(1)}) - \frac{1}{2} n_i h_{\nu\mu} \mathcal{N}^\mu \mathcal{N}^\nu, \qquad (B15)$$

where $P_{ij} = \delta_{ij} - n_i n_j$ is the projection operator. Multiplying both sides of Equation (B15) by $n^i$, we obtain

$$n^i \delta n_i = -n^i h_{\nu i}(0) \mathcal{N}^\nu - n^i \mathcal{N}_\mu \delta e^\mu_i$$
$$+ h_{\nu 0}(0) \mathcal{N}^\nu + \mathcal{N}_\mu \delta e^\mu_0 - \frac{1}{2} h_{\nu\mu} \mathcal{N}^\mu \mathcal{N}^\nu$$
$$= -n^i \mathcal{N}_\mu \delta e^\mu_i + \mathcal{N}_\mu \delta e^\mu_0 + \frac{1}{2} h_{\nu\mu} \mathcal{N}^\mu \mathcal{N}^\nu$$
$$= \mathcal{N}_\mu \mathcal{N}^\nu \delta e^\mu_\nu + \frac{1}{2} h_{\nu\mu} \mathcal{N}^\mu \mathcal{N}^\nu$$
$$= 0. \qquad (B16)$$

Note that in the last step, we use Equation (B12). Now, $n^i \delta n_i = 0$ shows that $\delta n_i$ is orthogonal to $n^i$, so we can multiply $P_{ij}$ to each term in the expression of $\delta n_i$, which reads

$$\delta n_i = -P_{ij}\left( \frac{1}{\omega_0} \kappa_j + h_{\nu j}(0) \mathcal{N}^\nu + \mathcal{N}_\mu \delta e^\mu_j \right). \qquad (B17)$$

Then we prove that this expression is gauge-invariant. Consider a transformation of coordinates $x'^\mu = x^\mu + \xi^\mu(x)$, which induces a gauge transformation of linearized theory:

$$h_{\mu\nu}(x) \rightarrow h_{\mu\nu}(x) - (\partial_\mu \xi_\nu(x) + \partial_\nu \xi_\mu(x)). \qquad (B18)$$

We check the gauge transformation of each term in $\delta n_i$. We use $\Delta$ to represent the change of each term after gauge transformation. Notice that $\Delta \Gamma^\rho_{\mu\nu} = -\partial_\mu \partial_\nu \xi^\rho$, $\Delta x^\mu(\lambda) = \xi^\mu(\lambda)$, so we have

$$\Delta \kappa^\mu = \frac{1}{\lambda_s}(\xi^\mu(\lambda_s) - \xi^\mu(0)$$
$$- \int_0^{\lambda_s} \int_0^{\lambda'} \partial_\gamma \partial_\nu \xi^\mu(\lambda'') k^\gamma_{(0)} k^\nu_{(0)} d\lambda'' d\lambda' \bigg)$$
$$= k^\nu_{(0)} \partial_\nu \xi^\mu(0) = \omega_0 \mathcal{N}^\nu \partial_\nu \xi^\mu(0). \qquad (B19)$$

In the rest of the discussion, we ignore the coordinate dependence of $\xi^\mu$, since now all the $\xi^\mu(\lambda)$ are defined on $\lambda = 0$. Here, we use $k^\nu_{(0)} \partial_\nu \xi^\mu = d\xi^\mu/d\lambda$ to simplify the integration.

From Equation (B10), we find

$$\partial_0(\Delta \delta e^\nu_i) = -\Delta \Gamma^\nu_{i0} = \partial_0 \partial_i \xi^\nu, \qquad (B20)$$

which means $\Delta \delta e^\nu_i = \partial_i \xi^\nu + f$. $f$ is an arbitrary function that has no dependence on time. We ignore $f$ because it is not correlated with gauge transformation. If we insert these expressions into $\delta n_i$, we can get the gauge transformation of

the angular deflection:

$$\Delta\delta n_i = -P_{ij}(\mathcal{N}^\nu\partial_\nu\xi_j - (\partial_j\xi_\nu + \partial_\nu\xi_j)\mathcal{N}^\nu$$
$$+ \mathcal{N}_\mu\partial_j\xi^\mu) = 0. \tag{B21}$$

Therefore, the angular deflection $\delta n_i$ is gauge-invariant. Now we choose a typical gauge to calculate $\delta n_i$. We use a synchronous gauge that is defined by $h_{00} = h_{0i} = 0$. The geodesic equations of the four-momentum of the detector are reduced to

$$\partial_0\delta e_\mu^\nu = -\Gamma_{\mu 0}^\nu = -\frac{1}{2}\partial_0 h_\mu^\nu, \tag{B22}$$

which gives

$$\delta e_\mu^\nu = -\frac{1}{2}h_\mu^\nu. \tag{B23}$$

For $\mu = 0$, $\delta e_0^\nu = 0$. Thus, the spatial components of the four-momentum of the detector do not contain first-order perturbations. Then we can treat the detector as a static object and $x^\mu(0)$ becomes a constant. Similarly, $x^\mu(\lambda_s)$ is also a constant, and they satisfy $x^\mu(\lambda_s) - x^\mu(0) = \lambda_s k_{(0)}^\mu$. The final expression of angular deflection is

$$\delta n_i = -P_{ij}\left(\frac{\eta_{j\mu}}{\omega_0\lambda_s}\int_0^{\lambda_s}\int_0^{\lambda'}\Gamma_{\gamma\nu}^\mu(\lambda')k_{(0)}^\gamma k_{(0)}^\nu d\lambda'd\lambda'\right.$$
$$\left.-\frac{1}{2}h_{jk}(0)n^k\right)$$
$$= -P_{ij}\left(\frac{\omega_0}{\lambda_s}\int_0^{\lambda_s}\int_0^{\lambda'}(-n^l\partial_0 h_{jl} + n^l n^k\partial_k h_{jl}\right.$$
$$\left.-\frac{1}{2}n^l n^k\partial_j h_{kl})d\lambda'd\lambda' - \frac{1}{2}h_{jk}(0)n^k\right). \tag{B24}$$

Using the identity

$$\frac{d}{d\lambda}h_{jl} = \omega_0(\partial_0 h_{jl} - n^k\partial_k h_{jl}), \tag{B25}$$

we can integrate the first two terms in Equation (B24):

$$\delta n_i = -P_{ij}\left(\frac{1}{\lambda_s}\int_0^{\lambda_s}(-n^l h_{jl}(\lambda') + n^l h_{jl}(0))d\lambda'\right.$$
$$\left.-\frac{\omega_0}{2\lambda_s}\int_0^{\lambda_s}\int_0^{\lambda'}n^l n^k\partial_j h_{kl}d\lambda''d\lambda' - \frac{1}{2}h_{jk}(0)n^k\right)$$
$$= -P_{ij}\left(-\frac{1}{\lambda_s}\int_0^{\lambda_s}n^l h_{jl}(\lambda')d\lambda'\right.$$
$$\left.-\frac{\omega_0}{2\lambda_s}\int_0^{\lambda_s}\int_0^{\lambda'}n^l n^k\partial_j h_{kl}d\lambda''d\lambda' + \frac{1}{2}h_{jk}(0)n^k\right). \tag{B26}$$

The angular deflection is separated into three terms:

$$\delta n_{1i} = \frac{1}{\lambda_s}P_{ij}\int_0^{\lambda_s}n^l h_{jl}(\lambda')d\lambda', \tag{B27}$$

$$\delta n_{2i} = \frac{\omega_0}{2\lambda_s}P_{ij}\int_0^{\lambda_s}\int_0^{\lambda'}n^l n^k\partial_j h_{kl}(\lambda'')d\lambda'd\lambda', \tag{B28}$$

$$\delta n_{3i} = -\frac{1}{2}P_{ij}h_{jk}(0)n^k. \tag{B29}$$

Now we estimate the relative size of these three terms. Without loss of generality, we consider the metric perturbation that takes the following form:

$$h_{ij}^{\mathrm{DP}}(\boldsymbol{x}, t) = c\mathcal{H}_{ij}^{\mathrm{DP}}\rho(\boldsymbol{x})\cos(2m_A t + 2\alpha), \tag{B30}$$

where $\mathcal{H}_{ij}^{\mathrm{DP}}$ is an order-one tensor and $\rho(\boldsymbol{x})$ refers to the local dark matter energy density, $c = -8\pi G/m_A^2$. For ultralight dark matter, a core structure can form at the center of the Galaxy with a radius of $\sim l_c = \lambda_{dB}/(2\pi) = 1/(m_A v_{\mathrm{vir}})$. The energy density of the core is a constant, which can be much larger than the energy density outside the core. We expect that a photon emitted by a star inside the core may have larger $\delta n_{1i}$ and $\delta n_{2i}$, since part of the worldline of the photon is inside the core. However, we will see in the following calculation that even when the star is inside the core, $\delta n_{3i}$ is still the dominant component of the total angular deflection $\delta n_i$.

### B.1. Earth Outside the Core, Star Inside the Core

Consider the case that the star is inside the core. It is valid for $l_s < \lambda_{\mathrm{dB}} = 2\pi l_c < l_e$ (with $l_e = 8$ kpc and $l_s$ being respectively the Earth and star's distance to the galactic center), implying $m_A \gtrsim 10^{-23.4}$ eV. We suppose that at $\lambda = \lambda_b$, the photon touches the boundary of the core. Therefore, we expect $\omega_0|\lambda_s - \lambda_b| \sim l_c$. First we calculate $\delta n_{1i}$. We separate $\delta n_{1i}$ into two parts:

$$\delta n_{1i} = \frac{c}{\lambda_s}P_{ij}\int_{\lambda_b}^{\lambda_s}n^l h_{jl}(\lambda')d\lambda' + \frac{c}{\lambda_s}P_{ij}\int_0^{\lambda_b}n^l h_{jl}(\lambda')d\lambda'. \tag{B31}$$

Since the $h_{ij}$ inside the core is significantly larger, we only calculate the first integration. In addition, the integral length is approximately one coherent length, so we can use Equation (B30) to express $h_{ij}$. Inserting Equation (B30) into $\delta n_{1i}$, we obtain

$$\delta n_{1i}^{\mathrm{DP}} = \frac{c}{\lambda_s}P_{ij}n^l\mathcal{H}_{jl}^{\mathrm{DP}}\int_{\lambda_b}^{\lambda_s}\rho(\lambda')\cos(2m_A\omega_0\lambda'$$
$$+ 2\alpha)d\lambda' \sim P_{ij}n^l\mathcal{H}_{jl}^{\mathrm{DP}}\frac{c\rho_c}{m_A\omega_0\lambda_s}, \tag{B32}$$

where $\rho_c$ refers to the energy density of the soliton core. For simplicity, we use the Navarro–Frenk–White (NFW) profile to estimate $\rho_c$. Suppose the energy density of DPDM near the Earth is $\rho_0$. The NFW profile takes the form (P. J. McMillan 2011)

$$\rho_h = \frac{\rho_{h,0}}{x(1 + x)^2}, \tag{B33}$$

where $x = r/r_h$ and $r_h = 17$ kpc. We use the energy density near $r = l_c$ to estimate the energy density of the core. Then the ratio of $\rho_c$ and $\rho_0$ is

$$\frac{\rho_c}{\rho_0} \sim \frac{l_e}{l_c} \sim l_e m_A v_{\mathrm{vir}}. \tag{B34}$$

Using the expression of $\rho_c$, we obtain

$$\delta n_{1i}^{\mathrm{DP}} \sim P_{ij} n^l \mathcal{H}_{jl}^{\mathrm{DP}} \frac{c\rho_0 v_{\mathrm{vir}} l_e}{x_s}$$
$$\sim c P_{ij} n^l \mathcal{H}_{jl}^{\mathrm{DP}} v_{\mathrm{vir}} \rho_0 \sim v_{\mathrm{vir}} \delta n_{3i}^{\mathrm{DP}}, \qquad (B35)$$

where $x_s$ is the distance from the star to the observer, $\delta n_{3i}^{\mathrm{DP}} = -\frac{1}{2} P_{ij} h_{jk}^{\mathrm{DP}}(0) n^k$. $l_e/x_s$ is an order-one parameter, so we ignore it. The virial velocity is $v_{\mathrm{vir}} \sim 10^{-3}$. Therefore, $\delta n_{1i}$ is suppressed compared to $\delta n_{3i}$.

Next we consider $\delta n_{2i}$. We exchange the order of integration in $\delta n_{2i}$, which yields

$$\delta n_{2i}^{\mathrm{DP}} = \frac{\omega_0}{2\lambda_s} P_{ij} \int_0^{\lambda_s} d\lambda'' \int_{\lambda''}^{\lambda_s} d\lambda' n^l n^k \partial_j h_{kl}^{\mathrm{DP}}(\lambda'')$$
$$= \frac{\omega_0}{2\lambda_s} P_{ij} \int_0^{\lambda_s} d\lambda'' (\lambda_s - \lambda'') n^l n^k \partial_j h_{kl}^{\mathrm{DP}}(\lambda'')$$
$$= \frac{\omega_0}{2\lambda_s} P_{ij} \int_{\lambda_b}^{\lambda_s} d\lambda'' (\lambda_s - \lambda'') n^l n^k \partial_j h_{kl}^{\mathrm{DP}}(\lambda'')$$
$$+ \frac{\omega_0}{2\lambda_s} P_{ij} \int_0^{\lambda_b} d\lambda'' (\lambda_s - \lambda'') n^l n^k \partial_j h_{kl}^{\mathrm{DP}}(\lambda''). \quad (B36)$$

Again, we only calculate the first integral. Inside the core, we find $\omega_0 |\lambda_s - \lambda''| \sim l_c = \frac{1}{m_A v_{\mathrm{vir}}}$ and $\partial_i h_{jk}^{\mathrm{DP}} \sim m_A v_{\mathrm{vir}} h_{jk}^{\mathrm{DP}}$. Then we have

$$\delta n_{2i}^{\mathrm{DP}} = \frac{\omega_0}{2\lambda_s} P_{ij} \int_{\lambda_b}^{\lambda_s} d\lambda'' (\lambda_s - \lambda'') n^l n^k \partial_j h_{kl}^{\mathrm{DP}}(\lambda'')$$
$$\sim \frac{1}{2\lambda_s} P_{ij} \int_{\lambda_b}^{\lambda_s} d\lambda'' \left( \frac{1}{m_A v_{\mathrm{vir}}} \right) n^l n^k m_A v_{\mathrm{vir}} h_{kl}^{\mathrm{DP}}(\lambda'')$$
$$\sim \frac{1}{2\lambda_s} P_{ij} \int_{\lambda_b}^{\lambda_s} d\lambda'' n^l n^k h_{kl}^{\mathrm{DP}}(\lambda'') \sim \delta n_{1i}^{\mathrm{DP}}, \qquad (B37)$$

where we find $\omega_0 (\lambda_s - \lambda'')$ and the spatial derivative of $h_{ij}^{\mathrm{DP}}$ cancel with each other, making $\delta n_{1i}^{\mathrm{DP}}$ and $\delta n_{2i}^{\mathrm{DP}}$ at the same order. Then, similar to $\delta n_{1i}^{\mathrm{DP}}$, $\delta n_{2i}^{\mathrm{DP}}$ is also suppressed compared to $\delta n_{3i}^{\mathrm{DP}}$.

### B.2. Both the Earth and the Star Are Inside the Core

We assume that the star and the Earth are inside the core. It requires $m_A < 10^{-23.4}$ to include the Earth inside the core. We treat the dark matter density at the core as a constant $\rho(\boldsymbol{x}) = \rho_c$. Then the first term $\delta n_{1i}$ in Equation (B29) has the approximated value

$$\frac{\delta n_{1i}^{\mathrm{DP}}}{\delta n_{3i}^{\mathrm{DP}}} \lesssim \frac{l_{\mathrm{Comp}}}{D} \sin\left( \frac{D}{l_{\mathrm{Comp}}} \right) \sim \begin{cases} l_{\mathrm{Comp}}/D, & l_{\mathrm{Comp}} \ll D \\ 1, & l_{\mathrm{Comp}} \gg D \end{cases}, \qquad (B38)$$

where $\omega_0 \lambda_s = D$ is the distance of the star and $1/m_A = l_{\mathrm{Comp}}$ is the Compton wavelength of the dark photon field. We find that $\delta n_{1i}$ is consistently smaller than $\delta n_{3i}$ when $l_{\mathrm{Comp}} \ll D$, which holds true for $m_A \gtrsim 10^{-24}$ eV with the typical star distance of 1 kpc. For $\delta n_{2i}^{\mathrm{DP}}$, we also easily find that it is at the same order of $\delta n_{2i}^{\mathrm{DP}}$, for the same reason we described in the previous subsection.

### B.3. Both the Earth and the Star are Outside the Core

Finally, we consider when the star and the Earth are outside the core. This is valid for a larger dark matter mass $m_A \gtrsim 10^{-23}$ eV, depending on the location of the star. Without loss of generality, we assume that the star lies on the line between the Earth and the galaxy center and the boundary of the core. Then, from previous sections, we have the dark matter density at the star $\rho_s = \rho_c \simeq \rho_0 l_c / l_e$ and

$$\frac{\delta n_{1i}^{\mathrm{DP}}}{\delta n_{3i}^{\mathrm{DP}}} \lesssim \frac{l_e}{l_c} \frac{l_{\mathrm{Comp}}}{D} \sin\left( \frac{D}{l_{\mathrm{Comp}}} \right) \sim \begin{cases} v_{\mathrm{vir}} l_e/D, & l_{\mathrm{Comp}} \ll D \\ l_e/l_c, & l_{\mathrm{Comp}} \gg D \end{cases}, \qquad (B39)$$

where we use $D \gg l_{\mathrm{Comp}}$, $l_c = v_{\mathrm{vir}} l_{\mathrm{Comp}}$, and $l_e \simeq 8$ kpc and $D \sim 1$ kpc. Similarly, $\delta n_{2i}^{\mathrm{DP}}$ is at the same order of $\delta n_{1i}^{\mathrm{DP}}$. As we estimated before, with the mass $m_A \geqslant 10^{-24}$ eV, we always have $l_{\mathrm{Comp}} \ll D$. Considering that $v_{\mathrm{vir}} \simeq 10^{-3}$, it is safe to ignore $\delta n_{1i}$ and $\delta n_{2i}$.

## ORCID iDs

Xiao Xue ● https://orcid.org/0000-0002-0740-1283

## References

Adshead, P., & Lozanov, K. D. 2021, PhRvD, 103, 103501
Afzal, A., Agazie, G., Anumarlapudi, A., et al. 2023, ApJL, 951, L11
Agazie, G., Anumarlapudi, A., Archibald, A. M., et al. 2023a, ApJL, 951, L8
Agazie, G., Anumarlapudi, A., Archibald, A. M., et al. 2023b, ApJL, 951, L50
Allen, B. 1996, in Relativistic Gravitation and Gravitational Radiation; Proc. of Les Houches School of Physics, ed. J.-A. Marck & J.-P. Lasota (Cambridge: Cambridge Univ. Press), 373
Amaral, D. W. P., Jain, M., Amin, M. A., & Tunnell, C. 2024, JCAP, 06, 050
Amin, M. A., Jain, M., Karur, R., & Mocz, P. 2022, JCAP, 08, 014
Antoniadis, J., Arumugam, P., Arumugam, S., et al. 2023, A&A, 678, A50
Aoyama, S., Yamauchi, D., Shiraishi, M., & Ouchi, M. 2021, arXiv:2105.04039
Armengaud, E., Palanque-Delabrouille, N., Yèche, C., Marsh, D. J. E., & Baur, J. 2017, MNRAS, 471, 4606
Arzoumanian, Z., Baker, P. T., Blecha, L., et al. 2023, ApJL, 951, L28
Belokurov, V., Erkal, D., Evans, N. W., Koposov, S. E., & Deason, A. J. 2018, MNRAS, 478, 611
Bini, D., & Geralico, A. 2018, PhRvD, 98, 124036
Blas, D., & Jenkins, A. C. 2022a, PhRvD, 105, 064021
Blas, D., & Jenkins, A. C. 2022b, PhRvL, 128, 101103
Boehm, C., Krone-Martins, A., Amorim, A., et al. 2017, arXiv:1707.01348
Book, L. G., & Flanagan, E. E. 2011, PhRvD, 83, 024024
Braginsky, V. B., Kardashev, N. S., Polnarev, A. G., & Novikov, I. D. 1990, NCimB, 105, 1141
Carroll, S. M. 2019, Spacetime and Geometry: An Introduction to General Relativity (Cambridge: Cambridge Univ. Press)
Çalışkan, M., Chen, Y., Dai, L., et al. 2024, JCAP, 05, 030
Chen, Y., Xue, X., Brito, R., & Cardoso, V. 2023, PhRvL, 130, 111401
Chowdhury, D., Hait, A., Mohanty, S., & Prakash, S. 2024, PhRvD, 110, 083023
Darling, J., Truebenbach, A. E., & Paine, J. 2018, ApJ, 861, 113
Dror, J. A., & Verner, S. 2024, arXiv:2406.03526
Fayet, P. 2018, PhRvD, 97, 055039
Fayet, P. 2019, PhRvD, 99, 055043
Garcia-Bellido, J., Murayama, H., & White, G. 2021, JCAP, 12, 023
González-Morales, A. X., Marsh, D. J. E., Peñarrubia, J., & Ureña López, L. A. 2017, MNRAS, 472, 1346
Guo, H.-K., Ma, Y., Shu, J., et al. 2019, JCAP, 05, 015
Haiman, Z., Xin, C., Bogdanović, T., et al. 2023, arXiv:2306.14990
Hlozek, R., Grin, D., Marsh, D. J. E., & Ferreira, P. G. 2015, PhRvD, 91, 103512
Hui, L., Ostriker, J. P., Tremaine, S., & Witten, E. 2017, PhRvD, 95, 043541
Jaraba, S., García-Bellido, J., Kuroyanagi, S., Ferraiuolo, S., & Braglia, M. 2023, MNRAS, 524, 3609
Kaiser, N., & Jaffe, A. 1997, ApJ, 484, 545
Kendall, E., & Easther, R. 2020, PASA, 37, e009

Khmelnitsky, A., & Rubakov, V. 2014, JCAP, 02, 019
Kim, H. 2024, PhRvD, 110, 083031
Klioner, S., Mignard, F., Lindegren, L., et al. 2021, A&A, 649, A9
Klioner, S. A. 2018, CQGra, 35, 045005
Kopeikin, S. M., & Makarov, V. V. 2006, AJ, 131, 1471
Kopeikin, S. M., Schafer, G., Gwinn, C. R., & Eubanks, T. M. 1999, PhRvD, 59, 084023
Liang, Q., Lin, M.-X., Trodden, M., & Wong, S. S. C. 2024, PhRvD, 109, 083028
Malbet, F., Boehm, C., Krone-Martins, A., et al. 2021, ExA, 51, 845
McMillan, P. J. 2011, MNRAS, 414, 2446
Mihaylov, D. P., Moore, C. J., Gair, J. R., Lasenby, A., & Gilmore, G. 2018, PhRvD, 97, 124058
Mihaylov, D. P., Moore, C. J., Gair, J. R., Lasenby, A., & Gilmore, G. 2020, PhRvD, 101, 024038
Moore, C. J., Mihaylov, D. P., Lasenby, A., & Gilmore, G. 2017, PhRvL, 119, 261102
Nelson, A. E., & Scholtz, J. 2011, PhRvD, 84, 103501
Nomura, K., Ito, A., & Soda, J. 2020, EPJC, 80, 419
O'Beirne, L., & Cornish, N. J. 2018, PhRvD, 98, 024020
Pardo, K., Chang, T.-C., Doré, O., & Wang, Y. 2023, arXiv:2306.14968
Pierce, A., Riles, K., & Zhao, Y. 2018, PhRvL, 121, 061102
Porayko, N. K., Zhu, X., Levin, Y., et al. 2018, PhRvD, 98, 102002
Prusti, T., de Bruijne, J. H. J., Brown, A. G. A., et al. 2016, A&A, 595, A1
Pyne, T., Gwinn, C. R., Birkinshaw, M., Eubanks, T. M., & Matsakis, D. N. 1996, ApJ, 465, 566
Qin, W., Boddy, K. K., & Kamionkowski, M. 2021, PhRvD, 103, 024045
Qin, W., Boddy, K. K., Kamionkowski, M., & Dai, L. 2019, PhRvD, 99, 063002
Raghavan, D., McAlister, H. A., Henry, T. J., et al. 2010, ApJS, 190, 1
Reardon, D. J., Zic, A., Shannon, R. M., et al. 2023, ApJL, 951, L6
Schive, H.-Y., Chiueh, T., & Broadhurst, T. 2014, NatPh, 10, 496
Sesana, A., Vecchio, A., & Colacino, C. N. 2008, MNRAS, 390, 192
Silverwood, H., & Easther, R. 2019, PASA, 36, e038
Simonetti, P., Vladilo, G., Silva, L., & Sozzetti, A. 2020, ApJ, 903, 141
Smarra, C., Goncharov, B., Barausse, E., et al. 2023, PhRvL, 131, 171001
Touboul, P., Metris, G., Rodrigues, M., et al. 2017, PhRvL, 119, 231101
Touboul, P., Metris, G., Rodrigues, M., et al. 2022, PhRvL, 129, 121102
Vallenari, A. 2018, FrASS, 5, 11
Vallenari, A., Brown, A. G. A., Prusti, T., et al. 2023, A&A, 674, A1
Wang, Y., Pardo, K., Chang, T.-C., & Doré, O. 2021, PhRvD, 103, 084007
Wang, Y., Pardo, K., Chang, T.-C., & Doré, O. 2022, PhRvD, 106, 084006
Weinberg, D. H., Bullock, J. S., Governato, F., Kuzio de Naray, R., & Peter, A. H. G. 2015, PNAS, 112, 12249
Wu, Y.-M., Chen, Z.-C., Huang, Q.-G., et al. 2022, PhRvD, 106, L081101
Xia, Z.-Q., Tang, T.-P., Huang, X., Yuan, Q., & Fan, Y.-Z. 2023, PhRvD, 107, L121302
Xu, H., Chen, S., Guo, Y., et al. 2023, RAA, 23, 075024
Xue, X., Xia, Z.-Q., Zhu, X., et al. 2022, PhRvR, 4, L012022
Yu, J.-C., Cao, Y., Tang, Y., & Wu, Y.-L. 2024, PhRvD, 110, 023025
Zwick, L., Soyuer, D., D'Orazio, D. J., et al. 2024, arXiv:2406.02306